Spin-wave-based tunable coupler between superconducting flux qubits

Shaojie Yuan,[1,2,*] Chuanpu Liu,[3,†] Jilei Chen,[1,‡] Song Liu,[1] Jin Lan,[4] Haiming Yu,[3,§] Jiansheng Wu,[1,‖] Fei Yan,[1] Man-Hong Yung,[1] Jiang Xiao,[5,¶] Liang Jiang,[6,**] and Dapeng Yu[1,††]

[1]*Institute for Quantum Science and Engineering, and Department of Physics, Southern University of Science and Technology, Shenzhen 518055, China*

[2]*Department of Physics, Yancheng Institute of Technology, Yancheng 224051, People's Republic of China*

[3]*Fert Beijing Research Institute, School of Electronic and Information Engineering, BDBC, Beihang University, 100191 Beijing, China*

[4]*Center of Joint Quantum Studies and Department of Physics, School of Science, Tianjin University, Tianjin 300350, China*

[5]*Department of Physics and State Key Laboratory of Surface Physics, Fudan University, Shanghai 200433, China*

[6]*Pritzker School of Molecular Engineering, The University of Chicago, Chicago, Illinois 60637, USA*

(Received 11 July 2022; accepted 23 December 2022; published 30 January 2023)

Quantum computing and simulation based on superconducting qubits have achieved significant progress and entered the noisy intermediate-scale quantum (NISQ) era recently. Using a third qubit or object as a tunable coupler between qubits is an important step in this process. In this article, we propose a hybrid system made of superconducting qubit and a yttrium iron garnet (YIG) system as an alternative way to realize this. YIG thin films have spin wave (magnon) modes with low dissipation and reliable control for quantum information processing. Here, we propose a scheme to achieve strong coherent coupling between superconducting (SC) flux qubits and magnon modes in YIG thin film. Unlike the direct $\sqrt{N}$ enhancement factor in coupling to the Kittel mode and other spin ensembles, with N the total number of spins, an additional spatial-dependent phase factor needs to be considered when the qubits are magnetically coupled with the magnon modes of finite wavelength. To avoid undesirable cancellation of coupling caused by the symmetrical boundary condition, a CoFeB thin layer is added to one side of the YIG thin film to break the symmetry. Our numerical simulation demonstrates avoided crossing and coherent transfer of quantum information between the flux qubit and the standing spin waves in YIG thin films. We show that the YIG thin film can be used as a tunable coupler between two flux qubits, which have a modified shape with small direct inductive coupling between them. Our results manifest that by cancellation of direct inductive coupling and indirect spin-wave couple of flux qubits we can turn on and off the net coupling between qubits. This bring magnonic YIG thin film into the field of quantum information processing.

DOI: 10.1103/PhysRevA.107.012434

I. INTRODUCTION

Quantum computing and simulation based on superconducting qubits have achieved significant progress and entered the noisy intermediate-scale quantum (NISQ) era in recent years [1–7]. Introduction of the tunable coupler is a breakthrough in this process [8–11]. It uses a central component as a coupler, which frequency tunes the virtual exchange interaction between two qubits and offsets the direct qubit-qubit coupling. This resolves many issues such as parasitic coupling between adjacent qubits and enables fast, high-fidelity two-qubit gates [8–11]. A tunable coupler based on a microwave scheme between flux qubits has been discussed [12,13]. In this work, we propose a schema using a hybrid quantum system made of superconducting qubits and a magnetic system as an alternative way to achieve this.

Many efforts have been devoted to hybridizing qubits with other physical systems, such as mechanical or magnetic systems [14–19]. For instance, the Kittel mode of a macroscopic yttrium iron garnet (YIG) sphere was coherently coupled to a transmon qubit in a three-dimensional (3D) cavity with the microwave photons manipulated inside the cavity [18]. Besides, the superconducting flux qubit was successfully hybridized with spin ensembles, i.e., nitrogen-vacancy (NV) centers in diamond via magnetic interaction [14–16]. On the other hand, because of the zero Joule heating, the wave nature with microwave working frequency, the spin wave (whose quanta is called magnon) has become a promising candidate for conventional information transmission and processing and has acquired the potential to establish a spin-wave-based computing technology, far beyond its complementary metal-oxide semiconductor (CMOS) counterpart [20–26]. Due to its favorably low damping, ferrimagnetic insulator YIG is particularly promising for these applications [27–29].

In this work, we propose a hybrid system consisting of superconducting flux qubits and the standing spin waves [30] in ferrimagnetic YIG thin film. The latter system has been widely used in spintronics and magnonics [27–29],

*416397255@qq.com
†chuanpu.liu@colostate.edu
‡chenjl6@sustech.edu.cn
§haiming.yu@buaa.edu.cn
‖wujs@sustech.edu.cn
¶xiaojiang@fudan.edu.cn
**liang.jiang@uchicago.edu
††yudp@sustech.edu.cn

 ©2023 American Physical Society

while its magnetic coupling to superconducting qubits and the corresponding application in quantum information processing has been rarely explored. As shown in the following, unlike the coupling to spin ensembles or the Kittel mode of spin waves [14,15,17], the enhancement factor for the coupling strength does not follow the $\sqrt{N}$ law, but carries a modulation associated with the finite spin-wave wavelength. In our proposal, an additional thin pinning layer of ferromagnetic CoFeB is deposited on one side of the YIG thin film to break the symmetry at the boundary conditions [31–39]. Avoided crossing of the energy spectrum can be numerically simulated by solving the Heisenberg equation based on the full Hamiltonian of the flux qubit, the spin waves in the YIG thin film, and their coupling. We find that it is possible to transfer quantum information coherently between the flux qubit and the spin wave mode in the YIG thin film. Moreover, we propose an experimentally feasible design to switch on and off the coupling between two shape-modified flux qubits or to entangle them via the perpendicular standing spin waves (PSSWs) of the YIG thin film. In this way, the interaction between flux qubits can be controlled via the spin wave modes and can be completely turned off without tuning to extremely large off resonance. .Hybridizing one flux qubit with and further "tuning" the net coupling between multiple flux qubits or entangling them through PSSWs highlights the application of a spin wave bus in quantum computing, further expanding the application of spin-wave-based computation technology [24,40–42].

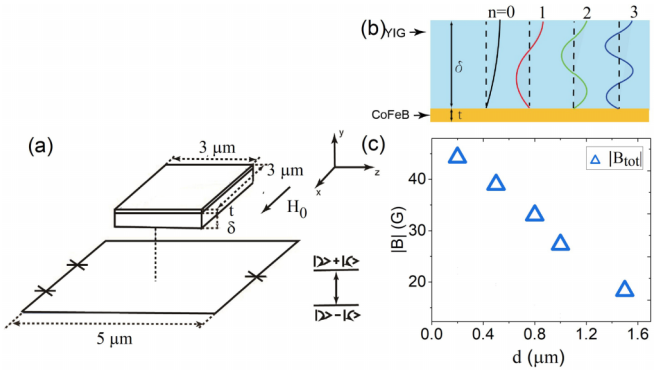

FIG. 1. Hybrid structure coupling a flux qubit and a YIG thin film (spin wave, or a magnon). (a) A YIG thin film with the dimension of $3\times0.08\times3$ μm^3 is placed in the center of the 5×5 μm^2 flux qubit loop separated by a distance d. An external field of 10 Gauss (H_0) is applied along the x axis. The thickness of the YIG thin film is $\delta_{\rm YIG} = 80$ nm and of the CoFeB capping layer is $t_{\rm CoFeB} = 10$ nm. The direction of the spins in both YIG and CoFeB for the ground state are along H_0 since the anisotropy fields for both materials are small and spin waves are perturbations of the spins from the ground state direction. (b) The PSSW of mode number $n = 0, 1, 2, 3$ with unsymmetrical boundary condition is depicted. The amplitude of PSSWs is zero at the interface since the spins are pinned. In our proposal, $n = 1$ mode is selected with wavelength $\lambda = 4\delta/3$ being excited. (c) Magnitude of total magnetic field on the flux qubit created by the YIG thin film and CoFeB thin layer.

II. HYBRID SYSTEM COUPLING SUPERCONDUCTING QUBITS AND SPIN WAVE

A superconducting (SC) loop with three Josephson junctions composes a flux qubit with the superposition of the clockwise and counterclockwise persistent current state as the qubit ground state $|g\rangle = |\circlearrowleft\rangle + |\circlearrowright\rangle$ and first excited state $|e\rangle = |\circlearrowleft\rangle - |\circlearrowright\rangle$ [43–45], respectively. The net currents and the resulting magnetic field threading the loop for the $|g\rangle$ and $|e\rangle$ states are distinct. Consequently, the Rabi oscillation between the two states of the flux qubit generates an alternating magnetic field perpendicular to the SC loop, which can be used to excite spin waves in the YIG system. The basic setup of the hybrid system is shown schematically in Fig. 1, which consists of a 5×5 μm^2 superconducting loop and a $3\times0.08\times3$ μm^3 YIG thin film above. A much thinner ferromagnetic CoFeB capping layer ∼10 nm in thickness is deposited on the top side of the YIG thin film to pin the magnetization in YIG at the interface. The magnetization follows the Dirichlet boundary condition at the pinned surface and the Neumann boundary condition at the other free surface [31–37]. The resonant frequencies of PSSW modes are [30]

$$f_{\rm PSSW} = \frac{\gamma\mu_0}{2\pi}\sqrt{\left[H_{\rm ext} + \frac{2A_{\rm ex}}{\mu_0 M_s}\left(\frac{n\pi}{\delta}\right)^2\right]\left[H_{\rm ext} + \frac{2A_{\rm ex}}{\mu_0 M_s}\left(\frac{n\pi}{\delta}\right)^2 + M_s\right]} \tag{1}$$

with gyromagnetic ratio $\gamma/2\pi = 28$ GHz/T, vacuum permeability $\mu_0 = 1.256\times10^{-6}$ N/A^2, saturation magnetization $M_s = 192$ kA/m for YIG, thickness $\delta = 80$ nm, exchange constant $A_{\rm ex} = 3.1$pJ/m, external field $H_{\rm ext}$, and mode number $n = 1, 2, 3, \ldots$. The experiment has measured the resonance value for the PSSW mode of 80-nm YIG thin film at near zero external field to be 4.57 GHz, which is different from the theoretical prediction of 3.39 GHz. The discrepancy may be due to choosing the order parameter to be the integer for unsymmetrical pinning in the fitting process, as actually there is 3/4 wavelength in the thickness direction for $n = 1$ as illustrated in Fig. 1(b). For our quantum control schemes, we will use the experimental resonance values and design a flux qubit with transition frequency close to $f_{\rm PSSW}^{(n=1)}$ and sufficiently detuned from the CoFeB resonance. Using geometric confinement, the proper boundary conditions, and a suitable coupling strength [see Eq. (4) with discussion)], the PSSW of wavelength of $\lambda = 4\delta/3 = (4\times80)/3$ nm can be excited. An external field of 10 Gauss is applied to align spins in YIG, and the total field created by YIG thin film and the CoFeB capping layer on the flux qubit is calculated and shown in Fig. 1(c), assuming the spin density $n_{\rm CoFeB} = 1.61\times10^{29}$ m^3 for CoFeB and $n_{\rm YIG} = 2.14\times10^{28}$ m^3 for YIG. The distance between the flux qubit and the YIG thin film is chosen to be around 1-1.5 μm for later simulation in Fig. 3. At these distances, the total magnetic field on the qubit is between

21.5 and 37 Gauss, which is less than the critical field of the aluminum superconductor (around 100 Gauss) and guarantees superconductivity of the flux qubit. In addition, other superconducting material such as Niobium can be used to fabricate the flux qubit, which has a much higher critical magnetic field for superconductivity, i.e., above 1000 Gauss.

From Ref. [30], the decay rates for YIG thin film and the CoFeB pinning layer are estimated as $\Gamma_{\mathrm{YIG},n=2} \sim 40$ MHz and $\Gamma_{\mathrm{CoFeB}} \sim 300$ MHz, where n is the PSSW mode number. Since the decay rate is proportional to the frequency and the frequency is approximately proportional to the square of the mode number, the intrinsic decay rate for the $n = 1$ PSSW mode is ∼10 MHz. The resonance frequency for the $n = 1$ PSSW mode in YIG thin film and the CoFeB pinning layer are $f_{\mathrm{YIG}} \sim 4.6$ GHz and $f_{\mathrm{CoFeB}} \sim 1.35$ GHz and the exchange coupling strength is $g_{\mathrm{CoFeB,YIG}} \sim 500$ MHz, obtained by the avoided crossing between the CoFeB Ferromagnetic resonance (FMR) and YIG PSSW in Ref. [30], which makes the converted decay rate of CoFeB on the $n = 1$ PSSW mode $\Gamma_{\mathrm{CoFeB}\to\mathrm{YIG},n=1} = (\frac{g_{\mathrm{CoFeB,YIG}}}{f_{\mathrm{YIG}}-f_{\mathrm{CoFeB}}})^2 \times 300 \sim 7$ MHz and the total decay rate for the $n = 1$ PSSW mode 17—20 MHz. In our proposal, we replace the microwave antenna in Ref. [30] with a flux qubit loop, which has a lower decay rate and a much smaller inductive coupling with the sample, and we expect the magnon decay rates will be further reduced. Therefore, it is reasonable to assume that the decay rate for the $n = 1$ PSSW mode is about 20 MHz.

In the following, we consider the coupling strength between the flux qubit and YIG thin film. The Hamiltonian for a ferromagnetic or ferrimagnetic material in a magnetic field takes the following general form [46]:

$$\hat{H} = -\sum_{m,n} J_{mn}\hat{\mathbf{S}}_m \cdot \hat{\mathbf{S}}_n + \sum_m \hat{\mathbf{S}}_m \cdot \mathbf{B}. \tag{2}$$

Here, $\hat{\mathbf{S}}_n$ is the spin operator on each site, which is along the x direction for the ground state in YIG thin film, and J_{mn} is the coupling matrix between spins. With the assumption that deviations from the group state are small, performing the Holstein–Primakoff approximation and transforming into the momentum space, we obtain

$$\hat{H} = -JNS^2 + NS\mu_B B_z + \sum_{\mathbf{k}}^{B.Z.}\sum_{i=1}^{3}(\hbar\omega_{k_i} + \mu_B B_z)a_{\mathbf{k}}^\dagger a_{\mathbf{k}} + \sum_{\mathbf{k}}^{B.Z.}\left[a_{\mathbf{k}}^\dagger \sum_m \left(\frac{2S}{N}\right)^{1/2} e^{i\mathbf{k}\cdot\mathbf{m}}\frac{B_x + iB_y}{2} + \mathrm{H.c.}\right], \tag{3}$$

where $i = 1, 2, 3$; $a_{\mathbf{k}}$ is the bosonic operator for spin waves in the momentum space; $\hbar\omega_{k_i} = 2JS(1 - \cos k_i) = 4JS\sin^2 k_i/2$; S is the total spin at each lattice site; $\mathbf{k}$ is the wave vector of the spin wave which is inversely proportional to the wavelength; and N is the number of lattice sites. In YIG thin film, different modes are spin waves with different wavelengths, and thus different wave vectors and resonance frequencies. From Eq. (3), by replacing the summation over each site with integration over space and inserting the spin density, the integral form of the coupling strength between the flux qubit and one mode of spin wave in YIG thin film is obtained as follows:

$$\frac{g_{\mathrm{eff}}^{\mathbf{k}}}{2\pi} \sim \frac{\sqrt{2S}\int \rho\mu_B e^{i\mathbf{k}\cdot\mathbf{r}}\frac{B_x+iB_y}{2}d^3\mathbf{r}}{\int \rho d^3 r}, \tag{4}$$

where $B_{x,y,z}$ is the microwave excitation field created by the flux qubit and ρ is the spin density in YIG. Unlike the simple $\sqrt{N}$ enhancement associated with coupling to the Kittel mode, there is an extra spatial-dependent phase factor $e^{i\mathbf{k}\cdot\mathbf{r}}$ in Eq. (4). For long wavelength spin wave, $|\mathbf{k}| \ll 1\ \mathrm{m}^{-1}$ and $e^{i\mathbf{k}\cdot\mathbf{r}} \sim 1$, and if B_x or B_y only vary slowly compared to $1/|\mathbf{k}|$ in real space, $g_{\mathrm{eff}}^{\mathbf{k}}$ will be proportional to $\sqrt{N}$. However, for the short wavelength spin wave, $g_{\mathrm{eff}}^{\mathbf{k}}$ is not necessarily proportional to $\sqrt{N}$ and can even be zero if the integration region covers exactly integer times of the wavelength along the wave vector direction. This is also the reason why, to excite the PSSW mode in YIG thin film by an almost homogenous field, an asymmetric boundary condition is required to avoid zero coupling strength caused by the phase factor. In our proposal, we mainly used the $n = 1$ PSSW mode of the YIG thin film. In-plane spin wave modes are also important in YIG thin films [47,48]. However, the in-plane magnetostatic surface wave-backward volume (MSSW-BV) modes will not interfere with our coupling scheme. The resonance frequency for the $n = 1$ PSSW mode in YIG thin film is 4.6 GHz. For the MSSW mode, the wavelength would be around 150 nm at the same frequency according to the dispersion, which is one order of magnitude smaller than the dimension of the micrometer-sized superconducting flux qubits. In this case, k would be large, and it would be very inefficient to directly excite spin waves with nanoscale wavelengths using flux qubits since there is a wavelength-scale phase factor in coupling strength formula in Eq. (4).

Given the dimension of the flux qubit square loop $5\times5\ \mu\mathrm{m}^2$ and the persistent current $I \sim 500$ nA [49,50], the magnetic field produced by the flux qubit can be evaluated using Ampere's law $B(\mathbf{r}) = \frac{\mu_0}{4\pi}\oint I\frac{d\mathbf{l}\times\mathbf{r}'}{|\mathbf{r}'|^3}$, and B_y dominates while B_x, B_z is close to zero in Fig. 1. Given a net spin density $\rho = 2.14\times10^{28}\ \mathrm{m}^{-3}$ in YIG, we obtain $|g_{\mathrm{eff}}^{\mathbf{k}}|$ as a function of the separation distance d between the flux qubits and $n = 1$ PSSW mode in the YIG thin film as in Fig. 2. Dash lines in Fig. 2 show the total decay rate of the flux qubit and $n = 1$ PSSW mode in YIG thin film containing both the intrinsic part and that influenced by the CoFeB thin layer. Decay rate for CoFeB is $\Gamma_{\mathrm{CoFeB}} \sim 300$ MHz, and the converted influence on the flux qubit from its electrons would be $\Gamma_{\mathrm{CoFeB}}\times(g/\Delta)^2 \sim 1.2$ MHz, where g is the coupling strength and Δ is the off resonance between the flux qubit and CoFeB. Coupling strength between the flux qubit and CoFeB thin layer g is obtained using Eq. (4), with long wavelength approximation ($k \sim 0$) and spin density of CoFeB being $1.61\times10^{29}\ \mathrm{m}^{-3}$ (Co). Here Fig. 2 is obtained based on theoretical calculations. In the future real experiment, flux qubits will be made on sapphire or silicon substrate, while YIG will be grown on gadolinium gallium garnet (GGG) substrate. A flip chip technique [51] can be used to assemble the two chips together. As indicated in Ref. [52], standoff distance between two chips of $2 - 20\ \mu$m has been achieved. We believe that by shortening the height of indium bump between the chips or even without using them, a smaller distance (e.g., 0.5 μm) can be obtained.

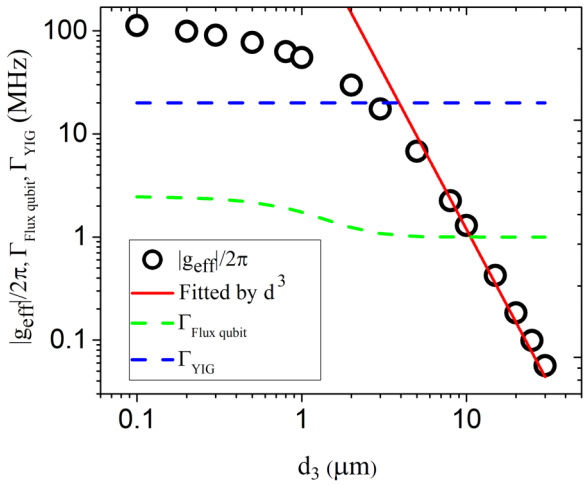

FIG. 2. Coupling strength $|g^{\mathbf{k}}_{\text{eff}}|$ and decay rate of the flux qubit and $n = 1$ PSSW in YIG, $\Gamma_{\text{flux qubit}}$, and Γ_{YIG} as a function of the separating spacing d. For small distance ($d < 2$ μm), $|g^{\mathbf{k}}_{\text{eff}}|$ for $k_y = 2\pi/\lambda$, where y is the direction in Fig. 1, decreases slowly with distance and is above 30 MHz, which is larger than the decay rate of magnon in YIG thin film. For large d, $|g^{\mathbf{k}}_{\text{eff}}|$ decreases as d^{-3}, indicated by the red curve. Two dash curves show decay rates for the YIG and flux qubit, Γ_{YIG} and $\Gamma_{\text{flux qubit}}$, as a function of separating spacing if YIG is deposited with CoFeB.

With the coupling strength estimated above, the full Hamiltonian with the flux qubit and YIG thin film can be written as

$$\hat{H} = -JNS^2 + NS\mu_B B_z + \sum_{\mathbf{k}}^{B.Z.} \sum_{i=1}^{3} (\hbar\omega_{k_i} + \mu_B B_z) a^{\dagger}_{\mathbf{k}} a_{\mathbf{k}} + \frac{\hbar}{2}(\Delta\sigma_x + \epsilon\sigma_z) - h\left[g^{\mathbf{k}}_{\text{eff}} a^{\dagger}_k + \left(g^{\mathbf{k}}_{\text{eff}}\right)^* a_k\right]\sigma_z + h\lambda\cos\omega t\,\sigma_z \tag{5}$$

where the first and second terms are the ferromagnetic and Zeeman terms, which can be neglected in the simulation for the reason that spin wave energy is a small perturbation compared to them; the third term describes the spin wave excitation; the fourth term is the flux qubit with Δ as the tunneling energy splitting and ϵ as the energy bias [53]; the fifth term characterizes the interaction between the two devices; and the last term is the external driving of the flux qubit. Here, $\sigma_{x,z}$ are the Pauli matrices. By changing the basis of the flux qubit, neglecting the Zeeman splitting and performing the rotating wave approximation, and then approximating the flux qubit as a harmonic oscillator, employing the Heisenberg relation, solving in Fourier space and transforming back to the lab frame (6), we obtain a simulation of the energy spectrum,

$$\tilde{\sigma}_{-,\omega} \sim \left[\omega - \sqrt{\Delta^2 + \epsilon^2} + i\Gamma_{fq} - \left|\frac{\Delta g^{\mathbf{k}}_{\text{eff}}}{\sqrt{\Delta^2 + \epsilon^2}}\right|^2 (\omega - \omega_{sw} + i\Gamma_{sw})^{-1}\right]^{-1}, \tag{6}$$

where ω is the driving pulse frequency and ω_{sw} is the resonance frequency of the standing spin wave of the YIG thin film. The expression of Eq. (6) describes the spectroscopic measurement of the flux qubit hybridized with one mode of spin waves in YIG thin film. Choosing parameters as $\Delta/2\pi = 4.52$ GHz, $\Gamma_{fq}/2\pi = 2$ MHz, $\omega_{sw}/2\pi = 4.57$ GHz, and $\Gamma_{sw}/2\pi = 20$ MHz, and letting $|g^{\mathbf{k}}_{\text{eff}}|/2\pi = 0$ and 30 MHz, we obtain a simulated spectrum for a bare qubit and a hybridized qubit-spin wave system, as shown in Fig. 3. Here, $\Gamma_{sw}/2\pi = 20$ MHz is a reasonable number since the decay rate for Kittel spin wave in a perfect sphere is around 1 MHz [17] and for finite wavelength spin wave in the YIG thin film is 6.8 MHz at 20 mK with GGG substrate and 1.4 MHz without substrate [54].The avoided crossing shows the strong coupling between the flux qubit and the $n = 1$ standing spin wave of YIG thin film with vacuum Rabi splitting $2g = 60$ MHz, which supports coherent energy or information exchange between them. Before preceding further, let us have a brief discussion about the capping CoFeB layer. We may introduce the damping constant $\alpha = \Gamma/f$, where α is the decay rate and f is the resonance frequency. For YIG, where α is on the order of 10^{-5}–10^{-4}, a low ferromagnetic alloy $Co_{25}Fe_{75}$ with damping constant as low as 5×10^{-4} is reported [55]. This material could substitute the CoFeB capping layer, which would have the decay rate $\Gamma_{\text{CoFeB}} < 1$ MHz instead of $\Gamma_{\text{CoFeB}} \sim 300$ MHz and decrease the total decay rate of the YIG-pinning layer to about 5 MHz. These further ensure the possibilities to implement thickness mode of YIG thin film in quantum information processing. It should be clarified that among the many k modes, only the $n = 1$ PSSW mode whose frequency matches the flux qubit will have anticrossing splitting with the qubit as in Fig. 3. Other modes also have coupling strength with the flux qubit according to Eq. (4). Since their frequencies are detuned from the flux qubit (0.435 GHz for $n = 0$ mode and 9.8 GHz for $n = 2$ mode), they will not have splitting with the flux qubit unless the frequency of the flux qubit is designed close to them. However, besides $n = 1$ mode, other modes will have effects for the tunable coupler, as will be discussed in the following section.

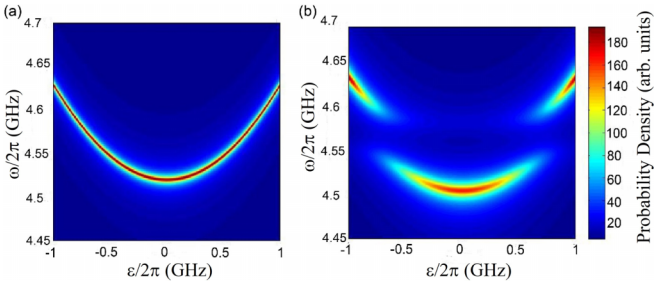

FIG. 3. Simulation of the energy spectrum of a flux qubit coupled to standing spin waves in the YIG thin film. (a) Spectrum of a bare flux qubit with $\Delta = 4.52$ GHz, $\Gamma_{fq} = 2$ MHz, and $g^{\mathbf{k}}_{\text{eff}} = 0$ in Eq. (7). (b) Spectrum of a flux qubit coupled to the standing spin wave of the flux qubit with $|g^{\mathbf{k}}_{\text{eff}}|/2\pi = 30$ MHz, $\omega_{sw}/2\pi = 4.57$ GHz, and $\Gamma_{sw}/2\pi = 20$ MHz.

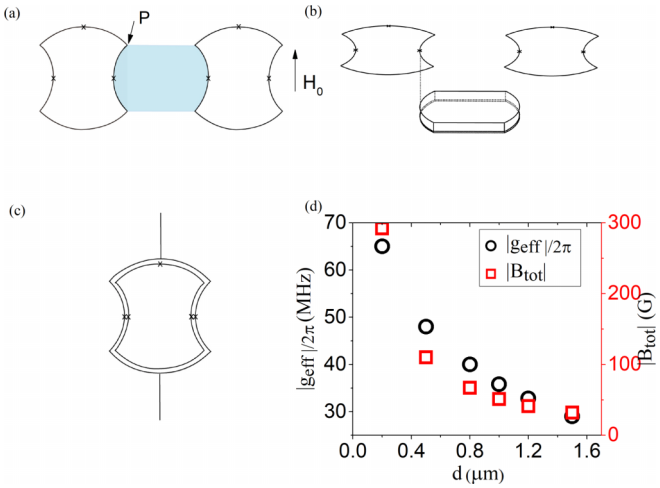

FIG. 4. Proposed setup for a tunable switch between two shape-modified flux qubits utilizing (with) YIG thin film. (a) Two shape-modified flux qubits are placed at a distance d above the 80-nm-thick YIG thin film, which is capped with a 10-nm CoFeB layer on one side. The special geometry of flux qubits is to decrease mutual inductance, and detailed dimensions of both flux qubits and YIG thin film are given in the context. (a) is top view and (b) is side view. (c) A special designed squid loop used for reading out the state of the flux qubit. (d) The absolute value of effective coupling strength (left axis) between one flux qubit and $n = 1$ PSSW mode in YIG thin film and the total magnetic field (right axis) at point p as in (a) created by the thin film as a distance of d. Coupling strength between the flux qubit and other modes can also be calculated according to Eq. (4). For a certain distance, coupling strength decreases as the mode number increases.

III. MAGNONIC TUNABLE COUPLER

In this section, we propose a scheme to entangle and further switch the coupling on and off between two shape-modified flux qubits through PSSW modes in YIG thin film. Figure 4 shows the schematic: two modified flux qubits with a center-to-center distance of $20\sqrt{2}$ μm are placed on top of a YIG thin film with a vertical separation d. The left/right arc of a flux qubit is a quarter of a 10-μm-radius circle and the top/down arc is a quarter of a 13.20-μm-radius circle. Mutual inductance of the two loops is given by the Neumann formula $L_{mn} = \frac{\mu_0}{4\pi}\oint\oint \frac{d\mathbf{X}_m d\mathbf{X}_n}{|\mathbf{X}_m - \mathbf{X}_n|}$. The designed orientations of those arcs are to decrease the mutual inductance between the two flux qubit loops from several tens of megahertz for comparable size square loops to 3.97 MHz for the current design with circulating current as much as 500 nA. YIG thin film is ∼80 nm in thickness with left/right sides being a quarter of a 10-μm circle and top/down sides having the length of $10\sqrt{2}$ μm, which is also deposited with 10 nm of CoFeB on one side. As oscillation occurs between the two states of a flux qubit, alternating magnetic fields are created outside the loop, and Fig. 4(d) shows the coupling strength between each flux qubit and the YIG thin film as a function of the distance d in between. As shown in Fig. 4, the stray magnetic field created by the YIG-CoFeB thin film is below the superconducting critical field of material of niobium, i.e., 1000 Gauss, that is used to fabricate the flux qubit. Here, the stray field is larger than that in Fig. 2 because the thin film is larger and closer to the flux qubits. As plotted in the graph, the external field is perpendicular to the direction of the three elements, and the ferromagnetic element (YIG) creates equal, static, and small flux for both flux qubits.

Readout of a flux qubit can be realized via another shape-modified squid loop as in Fig. 4(c). Mutual inductance between the squid loop and flux qubit is 3.8×10^{-11} H, while the one between the squid loop and the neighboring flux qubit is 5.6×10^{-14} H. This guarantees that the reading-out flux qubit will not be influenced much by the state of the neighboring qubit, even operating simultaneously. The microwave line, which is not shown, can quickly tune flux quit resonance frequency. At distance $d = 0.5$ μm, $|g^{\mathbf{k}}_{\text{eff}}|/2\pi$ are about 50 MHz for the $n = 1$ mode, 145 MHz for the $n = 0$ mode, and 23 MHz for the $n = 2$ mode by using Eq. (4) with different k substituted in. In our setup, the resonance frequencies are 0.435 GHz for the $n = 0$ mode, 4.57 GHz for the $n = 1$ mode, and 9.8 GHz for the $n = 2$ mode. If both flux qubits are detuned simultaneously to 4.32 GHz, effective coupling strength J between the two flux qubits can be

$$J \sim \frac{1}{2}g_{1,0}g_{2,0}\left(\frac{1}{\Delta_{1,0}}+\frac{1}{\Delta_{2,0}}\right)+\frac{1}{2}g_{1,1}g_{2,1}\left(\frac{1}{\Delta_{1,1}}+\frac{1}{\Delta_{2,1}}\right)+\frac{1}{2}g_{1,2}g_{2,2}\left(\frac{1}{\Delta_{1,2}}+\frac{1}{\Delta_{2,2}}\right). \tag{7}$$

Here, $g_{1,i}$, $g_{2,i}$, $\Delta_{1,i}$, and $\Delta_{2,i}$ are the coupling strength and detuning between flux qubits and each mode. This will cancel the mutual inductive coupling between (+3.97 MHz) the two flux qubit loops, thus switching off the coupling. On the other hand, if detuning both flux qubits to 400 MHz above 4.57 GHz, J would be 10.94 MHz, plus additional mutual inductive 3.97 MHz, so the total coupling strength would be about 15 MHz. Since the intrinsic lifetime for a flux qubit can be about 1 μs, a coupling strength of 15 MHz is strong enough to entangle the two qubits. In this way the coupling between two flux qubits is switched on and off. In addition, the intrinsic decay rate of $n = 1$ thickness mode spin wave in YIG thin film is about $\Gamma_{\text{YIG}} = 10$ MHz, which will introduce an extra broadening of $10\times(50/250)^2 = 0.4$ MHz on the flux qubit. Decay influence from other modes on the flux qubits will be much smaller, since they are far detuned. Similarly, the CoFeB thin layer gives rise to another $300\times(20/3300)^2 \sim 1$ MHz broadening on flux qubits, and if using $Co_{25}Fe_{75}$ this number could be as small as 0.02 MHz. It is possible to directly interact two flux qubits via mutual inductance and decrease inductive coupling between them by tuning them to off resonance, which is determined by $g_{\text{eff}} = g^2_{\text{mut}}/\Delta$, where g_{mut} is the mutual inductive coupling strength and Δ is the off resonance between them. For instance, for $g_{\text{mut}} = 10$ MHz, $g_{\text{eff}} = 1$ MHz, Δ is required to be 100 MHz; For $g_{\text{eff}} = 0.1$ MHz, Δ is required to be 1 GHz. In order to tune g_{eff} to an extremely small value, the off resonance Δ has to be extremely large and there is always a small reminiscent for g_{eff}. If utilizing YIG thin film as an adjustable coupler, inductive coupling can be directly tuned to approximately zero and there is no requirement for a large off resonance between qubits, but keeping the frequencies the same. In addition, for both entangling and tuning off coupling processes, YIG thin film is working in a dispersive regime. This suppresses the noise influence from the YIG thin film to flux qubits. Modes above $n = 2$ also have coupling strengths

with flux qubits. However, their frequencies will be much higher (above 9.8 GHz) according to Eq. (1) and the coupling strengths will be much smaller by using Eq. (4) due to smaller wavelengths and larger k. Thus, effective coupling between flux qubits through these modes will be one or two orders smaller than the main contributions from $n = 0, 1, 2$ modes, especially as n increases, and we did not consider them in Eq. (7). An external in-plane field of 10 Gauss is used to align the spins in YIG along one direction. The extra field used to tune the flux qubit is approximately 10 Gauss out of plane in the y direction in the tunable coupler scheme in Fig. 4, which will only slightly shift the resonance frequency of the PSSW mode. The hard axis of the magnetic YIG thin film is also out of plane in the y direction. Thus, this extra tuning field will not move the direction of spins out of plane much and they will mainly remain in the plane. This small external field will only slightly shift the resonance frequencies. For example, the gyromagnetic ratio is 28 GHz/T, and for a 10-Gauss field it created a shift of the resonance of 28 MHz. In addition, in the future real experiment, two flux qubits can be fabricated on the same silicon or sapphire substrate and YIG thin film will be on the GGG substrate on a different chip. They can be assembled together with the flip chip technique.

As demonstrated above, different from coupling to spin ensembles or the Kittel mode of spin waves, the coupling of the flux qubit with finite-wavelength (fundamental) spin wave mode has an extra phase term, which enables us to obtain the coupling strength and propose a scheme to hybridize flux qubit with a perpendicular standing spin wave in the YIG thin film. We further show that the PSSW spin wave mode in an YIG thin film can switch on and off the coupling between two flux qubits and generate entanglement. In short, by constructive and destructive interferences of direct inductive coupling and indirect coupling by spin waves, we can turn on and off the coupling between two flux qubits. This realizes the function of a tunable coupler.

IV. DISCUSSION AND CONCLUSION

A YIG sphere with low loss rate has been reported to couple with a transmon qubit via a microwave cavity. Our scheme is robust and different from them. First, YIG thin film is more widely used by the spin wave community. Second, a YIG sphere is usually millimeters in size in its coupling scheme, which is much larger than the micrometer-size flux qubit and is not suitable for the planar structure. In order to make the frequency of the Kittel mode of sphere match the transmon qubit, a large magnetic field has to be applied, and thus the sphere is usually several centimeters away from the transmon. This magnetic field will be large enough to destroy the superconductivity of the flux qubit if the YIG sphere and flux qubit are too close to each other. With the development of the film growth technique, the decay rate of the YIG thin film can approach 1 MHz for the substrate-free sample and 6 MHz for the sample with GGG substrate. When serving as a coupler, both the YIG thin film and CoFeB are working in a dispersive regime. This will cause less influence on the decay rate of the flux qubits. In addition, the CoFeB layer can be substituted with $Co_{25}Fe_{75}$, which has a much lower damping rate.

Our scheme used a third object to turn on and off the coupling between qubits, which is similar to other methods. It provides an alternative and useful option as a tunable coupler and combines fields of superconducting qubits and spin waves. More unique applications and strengths would be explored by using this hybrid system. In addition, fabrication of YIG thin film on the flux qubit could be a challenge in real experiment. A first attempt of experimental work that uses plasma focused ion beam (PFIB) technology to integrate YIG thin film with a superconducting microwave resonator has been reported [56]. The PFIB and flip chip techniques can also be implemented in a future experiment that transfers and integrates YIG thin film on the chip of the flux qubit.

In summary, we demonstrate two SC qubits coupled by spin waves through a hybrid system consisting of SC qubits and a magnetic system. We also manage to turn on and off the coupling between two flux qubits by constructive and destructive interferences of direct inductive coupling and indirect coupling induced by spin waves. This method provides an alternative way to achieve a tunable coupler and bridge a gap between magnonic YIG thin film and the field of quantum computation.

ACKNOWLEDGMENTS

The authors thank Huaiyang Yuan, Peihao Huang, and Xiuhao Deng for fruitful discussions. This work is supported by the Key-Area Research and Development Program of GuangDong Province (Grant No. 2018B030326001), the National Key Research and Development Program of China (Grant No. 2016YFA0300802), the National Natural Science Foundation of China (Grants No. 11704022, No. U1801661, and No. 12104208), the Guangdong Innovative and Entrepreneurial Research Team Program (Grant No. 2016ZT06D348), and the Science, Technology and Innovation Commission of Shenzhen Municipality (Grant No. KYTDPT20181011104202253).

[1] A. D. Córcoles, E. Magesan, S. J. Srinivasan, A. W. Cross, M. Steffen, J. M. Gambetta, and J. M. Chow, Nat. Commun. **6**, 6979 (2015).

[2] R. Barends, J. Kelly, A. Megrant, A. Veitia, D. Sank, E. Jeffrey, T. C. White, J. Mutus, A. G. Fowler, B. Campbell *et al.*, Nature (London) **508**, 500 (2014).

[3] M. Mirrahimi, Z. Leghtas, V. V. Albert, S. Touzard, R. J. Schoelkopf, L. Jiang, and M. H. Devoret, New J. Phys. **16**, 045014 (2014).

[4] A. Kandala, K. Temme, A. D. Cócoles, A. Mezzacapo, J. M. Chow, and J. M. Gambetta, Nature (London) **567**, 491 (2019).

[5] F. Arute, K. Arya, R. Babbush, D. Bacon, J. C. Bardin, R. Barends, R. Biswas, S. Boixo, F. G. S. L. Brandao, D. A. Buell *et al.*, Nature (London) **574**, 505 (2019).

[6] Y. Wu, W. Bao, S. Cao, F. Chen, M. Chen, X. Chen, T. Chung, H. Deng, Y. Du, D. Fan *et al.*, Phys. Rev. Lett. **127**, 180501 (2021).

[7] J. Preskill, Quantum **2**, 79 (2018).

[8] F. Yan, P. Krantz, Y. Sung, M. Kjaergaard, D. L. Campbell, T. P. Orlando, S. Gustavsson, and W. D. Oliver, Phys. Rev. Appl. **10**, 054062 (2018).

[9] M. C. Collodo, J. Herrmann, N. Lacroix, C. K. Andersen, A. Remm, S. Lazar, J. C. Besse, T. Walter, A. Wallraff, and C. Eichler, Phys. Rev. Lett. **125**, 240502 (2020).

[10] Y. Sung, L. Ding, J. Braumuller, A. Vepsalainen, B. Kannan, M. Kjaergaard, A. Greene, G.O. Samach, C. McNally, D. Kim *et al.*, Phys. Rev. X **11**, 021058 (2021).

[11] Y. Xu, J. Chu, J. Yuan, J. Qiu, Y. Zhou, L. Zhang, X. Tan, Y. Yu, S. Liu, J. Li *et al.*, Phys. Rev. Lett. **125**, 240503 (2020).

[12] R. Harris, A. J. Berkley, M. W. Johnson, P. Bunyk, S. Govorkov, M. C. Thom, S. Uchaikin, A. B. Wilson, J. Chung, E. Holtham *et al.*, Phys. Rev. Lett. **98**, 177001 (2007).

[13] S. H. W. van der Ploeg, A. Izmalkov, A. M. van den Brink, U. Hübner, M. Grajcar, E. Il'ichev, H.-G. Meyer, and A. M. Zagoskin, Phys. Rev. Lett. **98**, 057004 (2007).

[14] D. Marcos, M. Wubs, J. M. Taylor, R. Aguado, M. D. Lukin, and A. S. Sørensen, Phys. Rev. Lett. **105**, 210501 (2010).

[15] X. Zhu, S. Saito, A. Kemp, K. Kakuyanagi, S. Karimoto, H. Nakano, W. J. Munro, Y. Tokura, M. S. Everitt, K. Nemoto *et al.*, Nature (London) **478**, 221 (2011).

[16] X. Zhu, Y. Matsuzaki, R. Amsüss, K. Kakuyanagi, T. Shimo-Oka, N. Mizuochi, K. Nemoto, K. Semba, W. J. Munro, and S. Saito, Nat. Commun. **5**, 3524 (2014).

[17] Y. Tabuchi, S. Ishino, T. Ishikawa, R. Yamazaki, K. Usami, and Y. Nakamura, Phys. Rev. Lett. **113**, 083603 (2014).

[18] Y. Tabuchi, S. Ishino, A. Noguchi, T. Ishikawa, R. Yamazaki, K. Usami, and Y. Nakamura, Science **349**, 405 (2015).

[19] D. Lachance-Quirion, Y. Tabuchi, S. Ishino, A. Noguchi, T. Ishikawa, R. Yamazaki, and Y. Nakamura, Sci. Adv. **3**, e1603150 (2017).

[20] I. L. Markov, Nature (London) **512**, 147 (2014).

[21] Y. Kajiwara, K. Harii, S. Takahashi, J. Ohe, K. Uchida, M. Mizuguchi, H. Umezawa, H. Kawai, K. Ando, K. Takanashi *et al.*, Nature (London) **464**, 262 (2010).

[22] V. V. Kruglyak, S. O. Demokritov, and D. Grundler, J. Phys. D **43**, 264001 (2010).

[23] B. Lenk, H. Ulrichs, F. Garbs, and M. Müzenberg, Phys. Rep. **507**, 107 (2011).

[24] A. V. Chumak, V. I. Vasyuchka, A. A. Serga, and B. Hillebrands, Nat. Phys. **11**, 453 (2015).

[25] S. Dutta, S.-C. Chang, N. Kani, D. E. Nikonov, S. Manipatruni, I. A. Young, and A. Naeemi, Sci. Rep. **5**, 9861 (2015).

[26] W. Yu, J. Lan, and J. Xiao, Phys. Rev. Appl. **13**, 024055 (2020).

[27] T. Schneider, A. A. Serga, B. Leven, B. Hillebrands, R. L. Stamps, and M. P. Kostylev, Appl. Phys. Lett. **92**, 022505 (2008).

[28] A. V. Chumak, A. A. Serga, and B. Hillebrands, Nat. Commun. **5**, 4700 (2014).

[29] C. S. Davies, A. V. Sadovnikov, S. V. Grishin, Y. P. Sharaevsky, S. A. Nikitov, and V. V. Kruglyak, IEEE Trans. Magn. **51**, 1 (2015).

[30] H. Qin, S. J. Hämäläinen, and S. van Dijken, Sci. Rep. **8**, 5755 (2018).

[31] C. Kittel, Phys. Rev. **110**, 1295 (1958).

[32] P. E. Wigen, C. F. Kooi, M. R. Shanabarger, and T. D. Rossing, Phys. Rev. Lett. **9**, 206 (1962).

[33] R. F. Soohoo, Phys. Rev. **131**, 594 (1963).

[34] Y. S. Gui, N. Mecking, and C. M. Hu, Phys. Rev. Lett. **98**, 217603 (2007).

[35] R. Magaraggia, K. Kennewell, M. Kostylev, R. L. Stamps, M. Ali, D. Greig, B. J. Hickey, and C. H. Marrows, Phys. Rev. B **83**, 054405 (2011).

[36] S. Klingler, A. V. Chumak, T. Mewes, B. Khodadadi, C. Mewes, C. Dubs, O. Surzhenko, B. Hillebrands, and A. Conca, J. Phys. D **48**, 015001 (2015).

[37] M. A. W. Schoen, J. M. Shaw, H. T. Nembach, M. Weiler, and T. J. Silva, Phys. Rev. B **92**, 184417 (2015).

[38] S. Klingler, V. Amin, S. Geprägs, K. Ganzhorn, H. Maier-Flaig, M. Althammer, H. Huebl, R. Gross, R. D. McMichael, M. D. Stiles *et al.*, Phys. Rev. Lett. **120**, 127201 (2018).

[39] J. Chen, C. Liu, T. Liu, Y. Xiao, K. Xia, G. E. W. Bauer, M. Wu, and H. Yu, Phys. Rev. Lett. **120**, 217202 (2018).

[40] A. Khitun, M. Bao, and K. L. Wang, J. Phys. D **43**, 264005 (2010).

[41] G. Csaba, Á. Papp, and W. Porod, Phys. Lett. A **381**, 1471 (2017).

[42] J. Lan, W. Yu, R. Wu, and J. Xiao, Phys. Rev. X **5**, 041049 (2015).

[43] D. Abraham, J. Chow, A. Cócoles, M. Rothwell, G. Keefe, J. Gambetta, and M. Steffen, **27003** (2013).

[44] T. P. Orlando, J. E. Mooij, L. Tian, C. H. van der Wal, L. S. Levitov, S. Lloyd, and J. J. Mazo, Phys. Rev. B **60**, 15398 (1999).

[45] J. E. Mooij, T. P. Orlando, L. Levitov, L. Tian, C. H. van der Wal, and S. Lloyd, Science **285**, 1036 (1999).

[46] A. Altland, *Condensed Matter Field Theory*, 2nd ed. (Cambridge University Press, Cambridge, 2010).

[47] C. Liu, J. Chen, T. Liu, F. Heimbach, H. Yu, Y. Xiao, J. Hu, M. Liu, H. Chang, T. Stueckler *et al.*, Nat. Commun. **9**, 738 (2018).

[48] J. Chen, T. Yu, C. Liu, T. Liu, M. Madami, K. Shen, J. Zhang, S. Tu, M. S. Alam, K. Xia *et al.*, Phys. Rev. B **100**, 104427 (2019).

[49] J. Bylander, S. Gustavsson, F. Yan, F. Yoshihara, K. Harrabi, G. Fitch, D. G. Cory, Y. Nakamura, J. Tsai, and W. D. Oliver, Nat. Phys. **7**, 565 (2011).

[50] F. Yan, S. Gustavsson, A. Kamal, J. Birenbaum, A. P. Sears, D. Hover, T. J. Gudmundsen, D. Rosenberg, G. Samach, S. Weber *et al.*, Nat. Commun. **7**, 12964 (2016).

[51] C. R. Conner, A. Bienfait, H.-S. Chang, M.-H. Chou, É. Dumur, J. Grebel, G. A. Peairs, R. G. Povey, H. Yan, Y. P. Zhong, and A. N. Cleland, Appl. Phys. Lett. **118**, 232602 (2021).

[52] D. Rosenberg, D. Kim, R. Das, D. Yost, S. Gustavsson, D. Hover, P. Krantz, A. Melville, L. Racz, G. O. Samach, S. J. Weber, F. Yan, J. L. Yoder, A. J. Kerman, and W. D. Oliver, npj Quantum Inf. **3**, 42 (2017).

[53] I. Chiorescu, Y. Nakamura, C. J. P. M. Harmans, and J. E. Mooij, Science **299**, 1869 (2003).

[54] S. Kosen, A. F. van Loo, D. A. Bozhko, L. Mihalceanu, and A. D. Karenowska, APL Mater. **7**, 101120 (2019).

[55] M. A. W. Schoen, D. Thonig, M. L. Schneider, T. J. Silva, H. T. Nembach, O. Eriksson, O. Karis, and J. M. Shaw, Nat. Phys. **12**, 839 (2016).

[56] P. G. Baity, D. A. Bozhko, R. Macêdo, W. Smith, R. C. Holland, S. Danilin, V. Seferai, J. Barbosa, R. R. Peroor, S. Goldman *et al.*, Appl. Phys. Lett. **119**, 033502 (2021).